Unveiling the Dominant Control of the Systematic Cooling Bias in CMIP6 Models: Quantification and Corrective Strategies

Jie Zhang[1,2*], Kalli Furtado[3*], Steven T. Turnock[4,5], Yixiong Lu[1,2], Tongwen Wu[1,2], Fang Zhang[1,2], Xiaoge Xin[1,2], Yuyun Liu[6]

1. *State Key Laboratory of Disaster Weather Science and Technology, CMA EMPC*
2. *CMA Earth System Modeling and Prediction Centre, China Meteorological Administration, Beijing, China*
3. *Centre for climate research Singapore, Singapore*
4. *Met Office Hadley Centre, Exeter, UK*
5. *University of Leeds Met Office Strategic (LUMOS) Research Group, University of Leeds, Leeds, UK*
6. *Center for Monsoon System Research, Institute of Atmospheric Physics, Chinese Academy of Sciences, Beijing, China*

Corresponding to: Jie ZHANG (jiezhang@cma.gov.cn) & Kalli Furtado (Kalli_FURTADO@nea.gov.sg)

Abstract

Including sophisticated aerosol schemes in the models of the sixth Coupled Model Inter-comparison Project (CMIP6) has not improved historical climate simulations. In particular, the models underestimate the surface air temperature anomaly (SATa) when anthropogenic sulfur emissions increased in 1960-1990, making the reliability of the CMIP6 projections questionable. This cooling bias is largely attributable to the unreasonable simulated atmospheric sulfate burden changes. Sulfate burden anomaly are closely linked to both sulfate and SO_2 deposition processes. Intensified sulfate deposition directly reduces atmospheric sulfate loading, while enhanced SO_2 deposition limits precursor availability for sulfate formation by oxidation. These deposition processes regulate sulfate concentrations directly and indirectly. The systematically underestimated sulfate turnover time in CMIP6 models suggests that refining SO_2 deposition process rather than sulfate deposition would be a more scientific approach for model improvement. This is supported by two post-CMIP6 models that show better SATa reproduction after improving the SO_2 deposition parameterizations. Strong correlations between sulfate burden anomaly and SATa persist before, during, and after the 1960-1990 period. Such temporal consistency confirms the dominant role of sulfate-related physical processes across all examined time intervals.

1. Introduction

Atmospheric aerosols have rapidly increased since the Industrial Revolution. Over this time period, the total aerosol effective radiative forcing (ERF) was dominated by the sulfate cooling effect, and offset a substantial portion of global-mean forcing from well-mixed greenhouse gases (IPCC, 2023). Without this historical aerosol ERF, the Paris Agreement's target of limiting global warming to 1.5ºC above pre-industrial levels would have already been missed in 2015 (Hienola et al., 2018). Similarly, stopping all present-day anthropogenic aerosol emissions is estimated to induce a global-mean surface heating of 0.5-1.1ºC (Samset et al., 2018). The year 2024 has been confirmed as the hottest year in human history, and was the first year to breach the 1.5ºC warming limit (Bevacqua et al., 2025). Moreover, recent accelerated temperature trends may be attributable to reductions in atmospheric aerosols, particularly from reduced commercial shipping emissions. Hansen et al. (2025) suggest that even small emissions in relatively pristine air have substantial effects, highlighting the crucial need to improve the representation of aerosol effects in global climate models for more reliable projections.

The observed temporal evolution of historical surface air temperature (SAT) is one of the major metrics used for evaluating the performance of climate models. However, the SAT anomalies (SATa) in the CMIP6 models are systematically lower than was observed for the 1960-1990 period, whereas the CMIP5 models, on average, track the instrumental record quite well (e.g., Flynn and Mauritsen, 2020). The 1960-1990 period, when the cooling bias prevailed, is coincident with the so-called Great Acceleration period, during which human activities intensified remarkably and led to global-scale impacts on the Earth System (Steffen et al., 2007). Recent studies hypothesized that aerosol forcing in CMIP6 is stronger than in CMIP5 and is responsible for the suppressed late 20th-century warming (e.g., Dittus et al., 2020; Smith and Forster, 2021).

Given that all CMIP6 models use identical anthropogenic SO_2 emissions (Hoesly et al., 2018), the cooling anomaly points towards a problem with the sulfur cycle in recent

ESMs or the emissions data (Hardacre et al., 2021; Wang et al., 2021). In this study, we examine the sulfate-related processes in eleven CMIP6 models with aerosol schemes. We will identify the key processes governing sulfate burden in these models and provide recommendations for model further improvement.

2. Model, data, and method

2.1 CMIP6 models and data

Table 1. Information of the eleven CMIP6 models with aerosol schemes.

Model	Country	Interactive Chemistry	Members	Reference
BCC-ESM1	China	Yes	3	Wu et al., (2020); Zhang et al., (2021b)
CESM2	US	No	11	Danabasoglu et al. (2020)
CESM2-FV2	US	No	3	Danabasoglu et al. (2020)
EC-Earth3-AerChem	European consortium	Yes	2	Döscher et al. (2021)
GFDL-ESM4	US	Yes	3	Dunne et al. (2020)
MIROC6	Japan	No	50	Tatebe et al. (2019)
MIROC-ES2L	Japan	No	30	Hajima et al. (2020)
MPI-ESM-1-2-HAM	Germany	Yes	3	Mauritsen et al. (2019)
MRI-ESM2-0	Japan	Yes	10	Yukimoto et al. (2019)
NorESM2-LM	Norway	Yes	3	Seland et al. (2020)
UKESM1-0-LL	UK	Yes	19	Sellar et al. (2019)

Eleven CMIP6 climate models with interactive aerosol schemes are employed in this study, including seven models with interactive chemistry and four without (Table 1). The outputs from two CMIP6 experiments are used: (1) the historical experiment of climate change over the period 1850-2014, forced by time-varying external forcings that are based on observations of natural processes (e.g., solar activity, volcanic eruptions) and human-induced changes (e.g., greenhouse gas, aerosol emissions, land-use changes). All the available realizations for each model were used to minimize the uncertainty from internal variability in the climate system; (2) the 1pctCO2 simulations, in which CO_2 is gradually increased at a rate of 1% per year. The 1pctCO2 experiment is designed for studying model responses to CO_2 and is somewhat more realistic than rapidly increasing CO_2, such as in the abrupt-4×CO2 experiment. Historical experiment outputs from two post-CMIP6 models, BCC-ESM1-1 and UKESM1-1-LL, with revised SO_2 deposition parameterizations are also included in this study.

The model outputs used in this study include SAT and eight key sulfur-cycle variables: sulfate aerosol concentration, sulfate wet and dry deposition rates, sulfur dioxide concentration (SO_2), SO_2 wet and dry deposition rates, gas-phase and aqueous-phase oxidations of SO_2 to sulfate particles. For these sulfur-cycle variables, the inter-member variability within the historical experiment is substantially smaller than that of SAT. For instance, across the 11 CESM2 members, the standard deviation of sulfate burden is only about 4% of its interannual variability during 1960-1990, whereas the corresponding value for SAT is approximately 21%. Similar results are also evident in the 19 UKESM1 members, where the standard deviation of sulfate burden is 3% of its interannual variability, compared to 32% for SAT. Given that inter-member variability in sulfur-cycle variables is relatively small relative to their interannual fluctuations than SAT, we therefore use the first realization of the historical simulations and neglect inter-member differences for these sulfur-cycle variables.

Monthly mean SAT from the Met Office Hadley Centre/Climatic Research Unit global surface temperature dataset version 5 (HadCRUT5) from 1850 to 2014 are used for model evaluations (Morice et al., 2021). Considering the scarcity of long-term

reliable observations in polar regions, we focus on SAT changes within the latitudinal belt from 60°S to 65°N. The 'global' mean SAT is calculated as the area-weighted average over this latitudinal belt.

2.2 SO_2 turnover time and sulfate turnover time

Atmospheric sulfate concentrations are governed by the emission and oxidation of its precursors, as well as deposition processes. Anthropogenic SO_2 emissions are the major source of sulfate aerosol over land in polluted regions. Given that CMIP6 models typically employ identical anthropogenic SO_2 emission inventories, the inter-model spread in simulated sulfate concentrations primarily stems from discrepancies in SO_2-to-sulfate oxidation rates and sulfate deposition velocities. Here we define the atmospheric residence time of SO_2 and sulfate aerosols as follows.

SO_2 turnover time is determined by its atmospheric burden and its total loss rate, which includes both deposition and chemical oxidation to sulfate. It is defined as:

$$\tau_{SO_2} = \frac{B_{SO_2}}{(R_{dSO_2} + R_{oSO_2})} \quad (2),$$

where τ_{SO_2} is the SO_2 turnover time, B_{SO_2} is the global mean atmospheric SO_2 burden, R_{dSO_2} is the total SO_2 deposition rate including both wet and dry depositions, and R_{oSO_2} is the oxidation rate of SO_2 to sulfate via gas-phase and aqueous-phase chemistry.

Sulfate turnover time is defined as:

$$\tau_{SO_4} = \frac{B_{SO_4}}{R_{dSO_4}} \quad (1),$$

where τ_{SO_4} is the sulfate turnover time, B_{SO_4} is the global mean atmospheric sulfate burden, and R_{dSO_4} is the global mean total sulfate deposition rate including both wet and dry depositions.

2.3 The transient Climate Response (TCR) index

The Transient Climate Response (TCR) index is calculated as the mean SAT anomaly over a 20-year period centered on the year when atmospheric CO_2 concentration has doubled in the 1pctCO2 simulation. It is an important metric for quantifying CO_2-induced historical warming and has been widely used for model evaluations and intercomparison studies (e.g., Bevacqua et al., 2025; O'neill et al., 2016).

3. Results

3.1 SATa and sulfate burden anomaly

The historical evolutions of global mean SATa in the eleven CMIP6 models with interactive aerosol schemes are shown in Fig. 1a. All the models tend to underestimate SATa since the 1930s. The cooling anomaly in CMIP6 model marked a notable departure from earlier model generations, which can effectively capture the instrumental SAT record with observation falling well within model spread (e.g., Flynn and Mauritsen, 2020; Hegerl, et al., 2007).

The cooling bias is most pronounced from 1960 to 1990. The SATa is about 0.34ºC in the observations. However, the multi-model mean (MMM) SATa is about 0.3ºC lower with a large model spread. The SATa ranges from -0.24ºC in EC-Earth3-AerChem to 0.19ºC in GFDL-ESM4 and MIROC6. The cooling is noticeable at the mid to high latitude in the Northern Hemisphere (as shown in the attached SATa map in Fig.1a). The sudden drop in SATa in the early 1960s and 1990s may be due to the stronger model responses to large volcanic eruptions, Mount Agung in 1963 and Mount Pinatubo in 1991, than in the observations (Chylek et al., 2020). The cooling biases diminish in later periods corresponding to the generally high model sensitivity to greenhouse gas forcing (Smith and Forster, 2021).

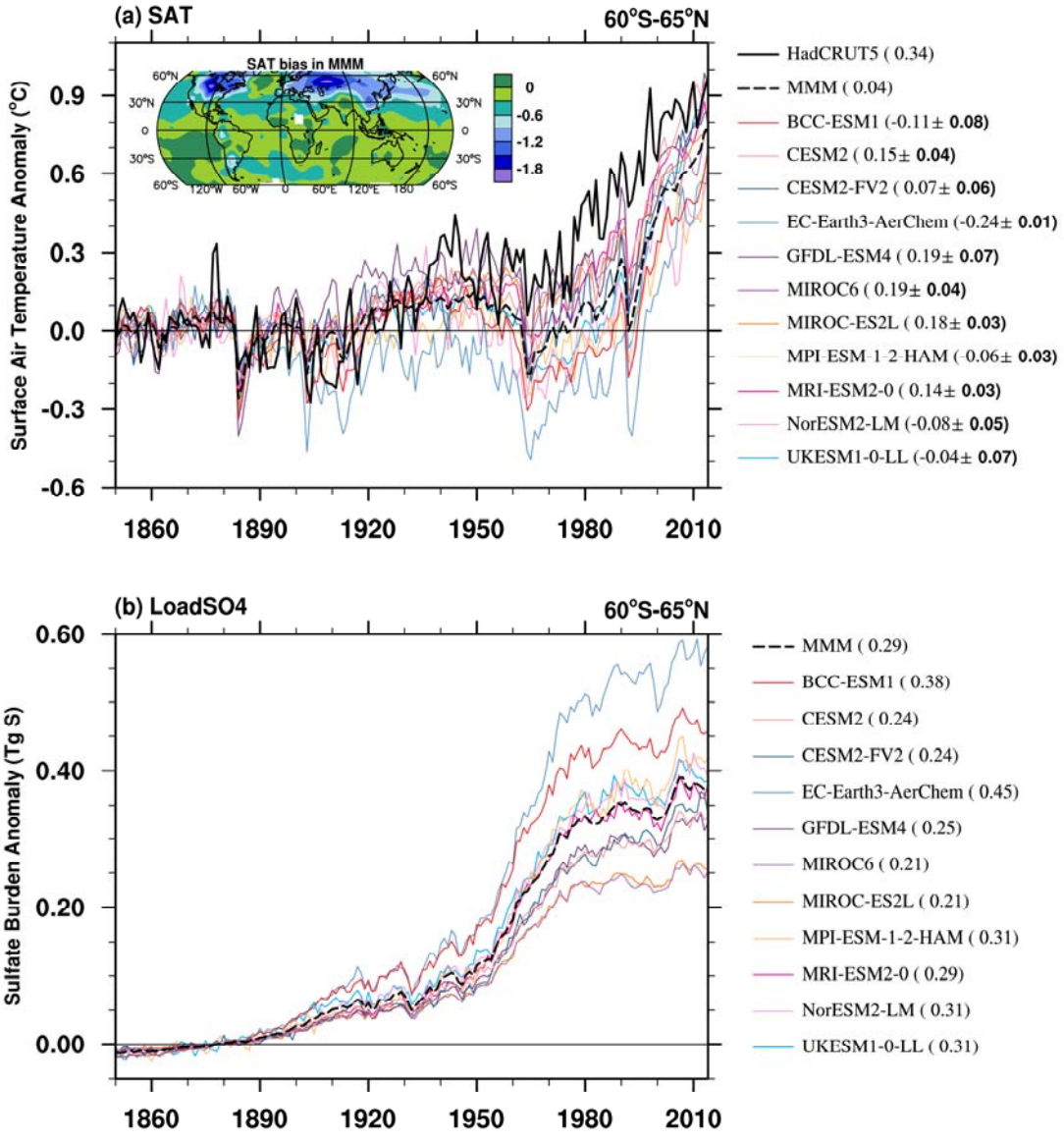

Figure 1. (a) Historical surface air temperature anomalies (SATa) relative to 1850-1900 mean from HadCRUT5 (thick black line), the ensemble mean of each CMIP6 model (solid colored lines), and the multi-model mean (MMM; dashed black line). Numbers in parentheses indicate the mean SATa for each model during 1960-1990, with the inter-member spread shown as ± one standard deviation. Units: ºC. (b) Same as (a), but for sulfate burden anomalies for the first realization of each CMIP6 model (colored lines) and the MMM (dashed black line). Units: Tg S.

The cooling bias in CMIP6 models coincides with the rapidly increase in anthropogenic emissions, particularly of SO_2, the primary precursor of atmospheric sulfate (Zhang et al., 2021a). Global SO_2 emissions grew steadily after the 1950s and peaked in the 1970s at approximately 180Tg yr^{-1}, about 3.6 times the level of the 1950s (Hoesly et al., 2018). The rise in SO_2 emissions has directly contributed to elevated

sulfate concentrations in the troposphere. The temporal evolution of sulfate burden shows significant upward trend align with the anthropogenic emission (Fig.1b), initially driven by industrialization and further accelerated after the 1950s mainly due to intensified anthropogenic SO_2 emission from industries and the energy-transformation sectors (e.g., Ohara et al., 2007; Vestreng et al., 2007). The increased sulfate burden interrupted a decades-long warming trend through the cooling effect of sulfate aerosols, even as atmospheric CO_2 concentrations continued to rise (Wilcox et al., 2013).

Due to emission-control policies implemented in Europe and North America (Aas et al., 2019; Hand et al., 2012; Vestreng et al., 2007), such as the Gothenburg Protocol (Eb, 1999) and the 1990 Clean Air Act Amendments in the U.S. (Likens et al., 2001), global anthropogenic SO_2 emissions were suppressed after the 1980s and SAT started to rise rapidly in both observation and model simulations. It should be noted that the CMIP6 emission inventory does not fully capture the early 21st century SO_2 emission reductions in East Asia (Wang et al., 2021). However, this period lies outside the 1960-1990 focus of the present study, and its impact on SAT reproduction is beyond the main scope of this paper.

The systematically underestimated SATa suggests an excessively strong sulfate-induced cooling effect in CMIP6 models, as indicated by the contrasting performance of individual models. For instance, the MIROC models exhibit the lowest sulfate burden (0.21 Tg S) and smallest cooling bias relative to observation (0.15°C below HadCRUT5), while EC-Earth3-AerChem generate a sulfate burden approximately doubles that value (0.45 Tg S) and nearly four times the cooling bias (0.58°C below HadCRUT5). Analysis across the 11 CMIP6 models reveals a statistically significant negative correlation of -0.92 between sulfate burden anomalies and SATa underestimation during 1960-1990 (Fig. 2a). This relationship highlights the potential role of overestimated sulfate-induced cooling in driving the inter-model spread of SATa biases.

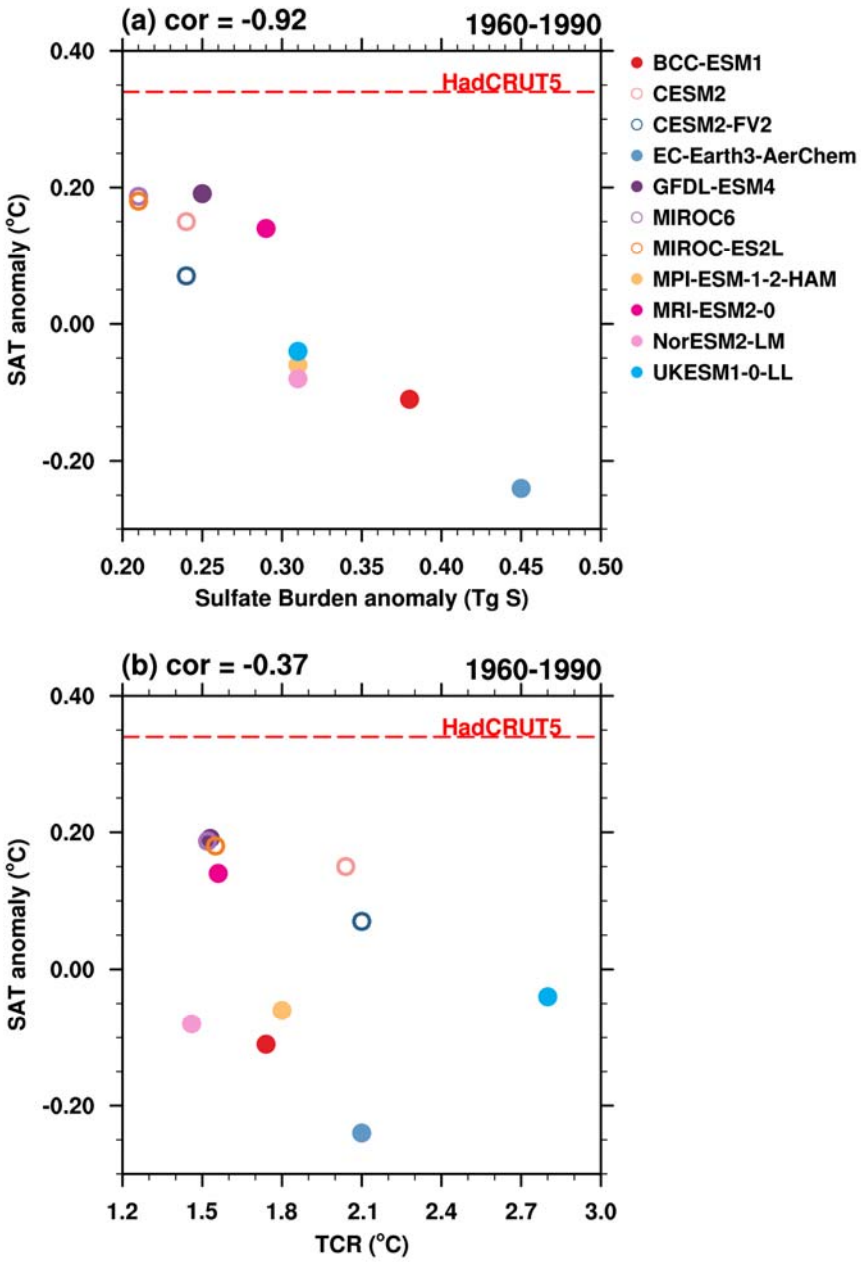

192

193 **Figure 2.** (a) Scatter plots sulfate burden anomaly versus SATa during 960-1990 from historical
194 experiments. (b) Scatter plot of TCR versus SATa during 1960-1990. Anomalies are calculated
195 relative to the 1850-1900 mean. Models with and without interactive chemistry are denoted by
196 colored dots and colored circles, respectively. The corresponding correlation coefficient (cor) for
197 each panel is shown in the upper-left corner.

198 Interactive chemistry may affect sulfate formation and sulfate aerosol burdens in
199 the atmosphere (Mulcahy et al., 2020). Models with interactive chemistry (colored dots
200 in Fig.2a) generally show higher sulfate burdens and lower SATa than non-interactive
201 models (colored circles). However, the relationship between sulfate burden anomaly

and SATa is a robust feature across CMIP6 models, independent of their chemical complexity.

Greenhouse gases (GHGs) also increased rapidly during 1960-1990. However, TCR, which can generally indicate the impact of GHGs, is insignificantly correlated with SATa in CMIP6 models, and the correlation coefficient across models is even negative (Fig.2b). Therefore, the inter-model spread in cooling biases can substantially be attributed to discrepancies in simulated sulfate aerosol burden.

It should be noticed that there are fast and slow components of global warming in response to radiative forcing changes (Held et al., 2010). The fast component, characterized by an exponential decay timescale of less than 5 years, is primarily driven by rapid adjustments in the upper ocean layers. In contrast, the slow component evolves over centuries and is associated with heat uptake by deeper ocean layers. Lagged oceanic and dynamical feedbacks will further delay and modulate warming rates (Chen et al., 2016; Watterson and Dix, 2005). In this study, the fast response to sulfate forcing can be rapidly detected by SATa, especially when the sulfate forcing is sustained during 1960-1990. Moreover, the global mean perspective in this study makes the results insensitive to the impact of spatial redistribution of temperature anomalies caused by dynamical feedbacks.

3.2 Sulfur Deposition rates and SO_2 oxidation rate

SO_2 deposition, sulfate deposition, and SO_2 oxidation to sulfate are the key processes governing the atmospheric sulfur cycle. About half of the SO_2 emission is removed by dry deposition at surface and through wet scavenging by precipitation (e.g., Chin et al., 1996). The remaining fraction is oxidated to sulfate, mainly through two pathways: gas-phase reaction with the hydroxyl radical (OH), and aqueous-phase oxidation within cloud and fog droplets, where reactions with ozone (O_3) and hydrogen peroxide (H_2O_2) are dominant. These processes are critical determinants of atmospheric sulfate burden.

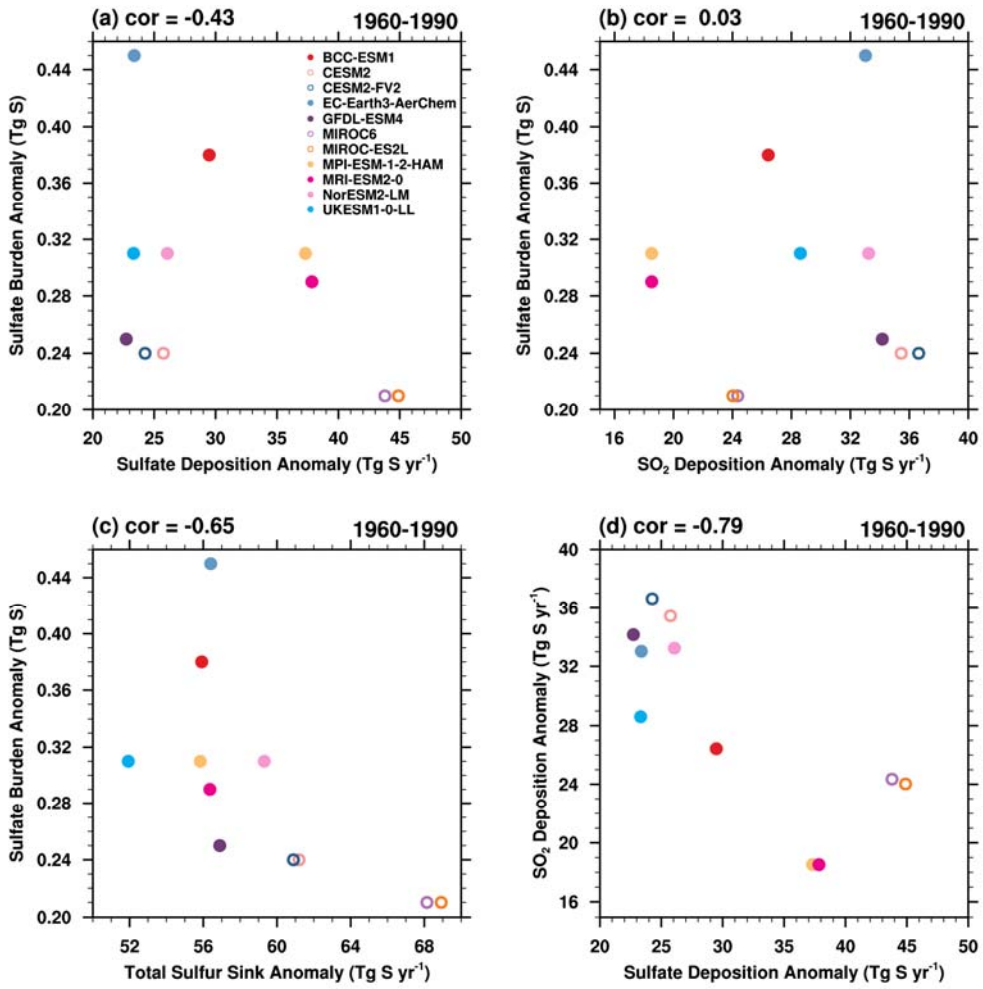

230

231 **Figure 3.** (a) Sulfate deposition anomaly, (b) SO_2 deposition anomaly, and (c) total sulfur sink
232 anomaly versus sulfate burden anomaly (Tg S, y-axis) in each model during 1960-1990. (d) Sulfate
233 deposition anomaly (x-axis) versus SO_2 deposition anomaly (y-axis) during 1960-1990. Units for
234 deposition anomalies are Tg S yr^{-1}.

235 Fig. 3 shows the inter-model relationship between global mean anomalies of
236 sulfate burdens and sulfur depositions during 1960-1990, relative to the pre-industrial
237 baseline (1850-1900). The sulfate burden anomaly is negatively correlated with sulfate
238 deposition anomaly. However, the correlation is statistically insignificant. This may be
239 partly attributable to a subset of five models characterized by both low sulfate burden
240 and low sulfate deposition anomalies. These models degrade the robustness of the linear
241 fit derived from the remaining models. There is no clear statistical relationship between
242 sulfate burden anomaly and SO_2 deposition anomaly (Fig. 3b). However, when
243 considering the total sulfur sink anomaly, including both sulfate and SO_2 deposition

anomalies, the correlation with sulfate burden anomaly strengthens to -0.65, significant at the 5% level using a Student's t-test (Fig.3c). Notably, within the subset of five models, most show higher SO_2 deposition anomaly in relative to the multi-model mean. This high SO_2 deposition anomaly compensates for their low sulfate deposition anomaly, influencing the total sulfur deposition magnitude sufficiently to sustain a significant correlation with sulfate burden anomaly in these models. Further analysis reveals a strong negative correlation (-0.79) between SO_2 deposition rate anomaly and sulfate deposition rate anomaly, suggesting a compensatory relationship between these two sulfur removal pathways (Fig.3d).

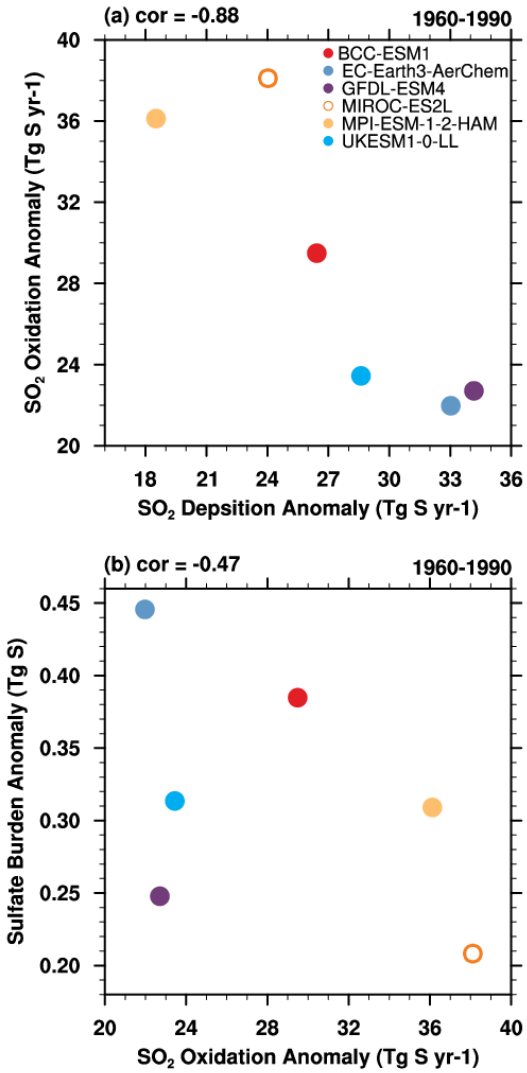

Figure 4. (a) SO_2 deposition anomaly versus SO_2 oxidation anomaly, and (b) SO_2 oxidation anomaly versus sulfate burden anomaly in each model during 1960-1990.

The formation of atmospheric sulfate aerosol is governed by the balance between the loss of its precursor, SO_2, and its chemical transformation. As shown in Fig.4a, inter-model comparisons show a significant anti-correlation between SO_2 deposition anomaly and the oxidation rate anomaly across the six models for which relevant data are available for calculation (-0.88). That is, enhanced SO_2 deposition rate, particularly through dry deposition processes, limits the availability of SO_2 for oxidation to sulfate. The relationship between oxidation rate anomalies and the sulfate burden anomalies is negative but not statistically robust within this limited model subset. A more comprehensive analysis with a larger model ensemble is needed to robustly quantify the relative contributions of oxidation pathways to the sulfate aerosol burden.

Therefore, biases in sulfate burden simulations arise either directly from sulfate deposition or indirectly from SO_2 deposition, which limits the availability of SO_2 for oxidation.

3.3 SO_2 turnover time and sulfate turnover time

SO_2 deposition, sulfate deposition, and SO_2 oxidation rate determine the respective turnover times for SO_2 and sulfate, which quantify their mean atmospheric residence times before removal. Here we examine SO_2 turnover time and sulfate turnover time, quantities with clear physical interpretations, to identify the dominant physical and chemical processes responsible for the sulfate burden biases.

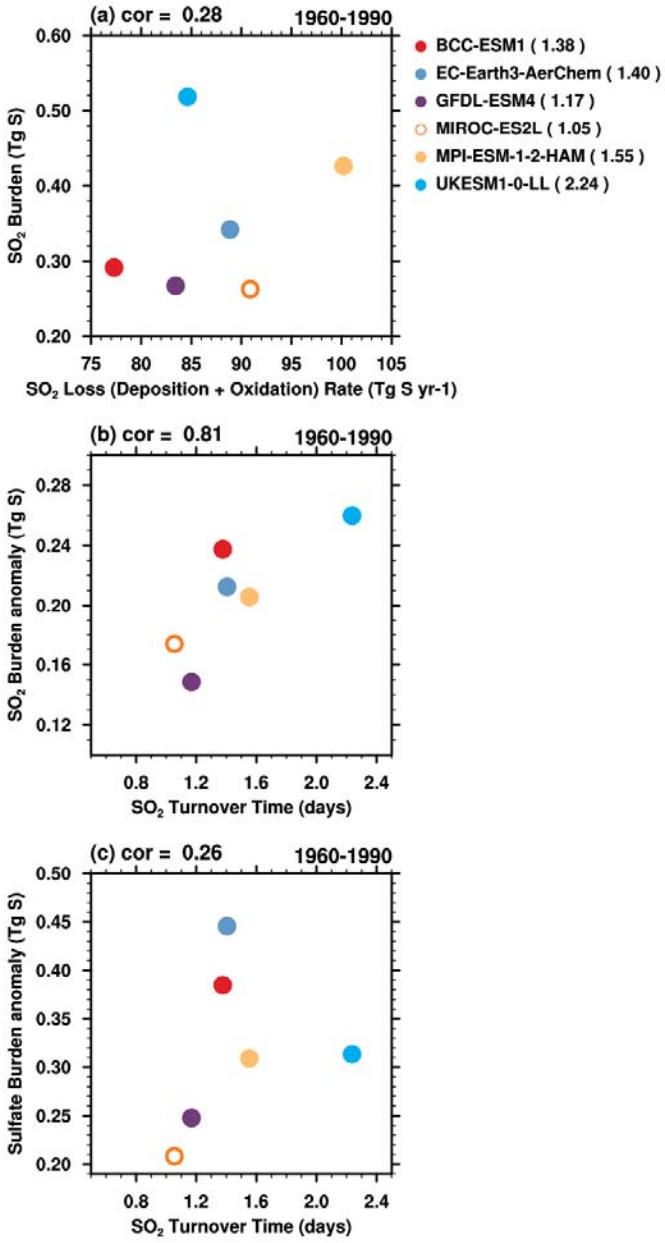

Figure 5. (a) SO_2 loss rate versus SO_2 burden in 1960-1990. SO_2 loss rate includes SO_2 deposition and oxidation. (b) SO_2 turnover time versus SO_2 burden anomaly in 1960-1990. (c) SO_2 turnover time versus SATa in 1960-1990.

The correlations between SO_2 burden and its total loss rate, including both deposition and chemical oxidation, are notably weak (Fig.5a). Given that the models share identical anthropogenic SO_2 emission inventories, this poor correlation likely stems from substantial inter-model differences in the representation of natural SO_2 precursor emissions (e.g., from oceanic dimethyl sulfide) and their subsequent

atmospheric processing. The SO_2 turnover time (τ_{SO_2}) as defined in Eq. 1, ranges from 1.05 to 2.24 days in the CMIP6 models. The τ_{SO_2} is highly correlated with SO_2 burden anomaly with correlation coefficient of 0.81 (Fig.5b). However, its correlation with the sulfate burden anomaly is weak (Fig.5c).

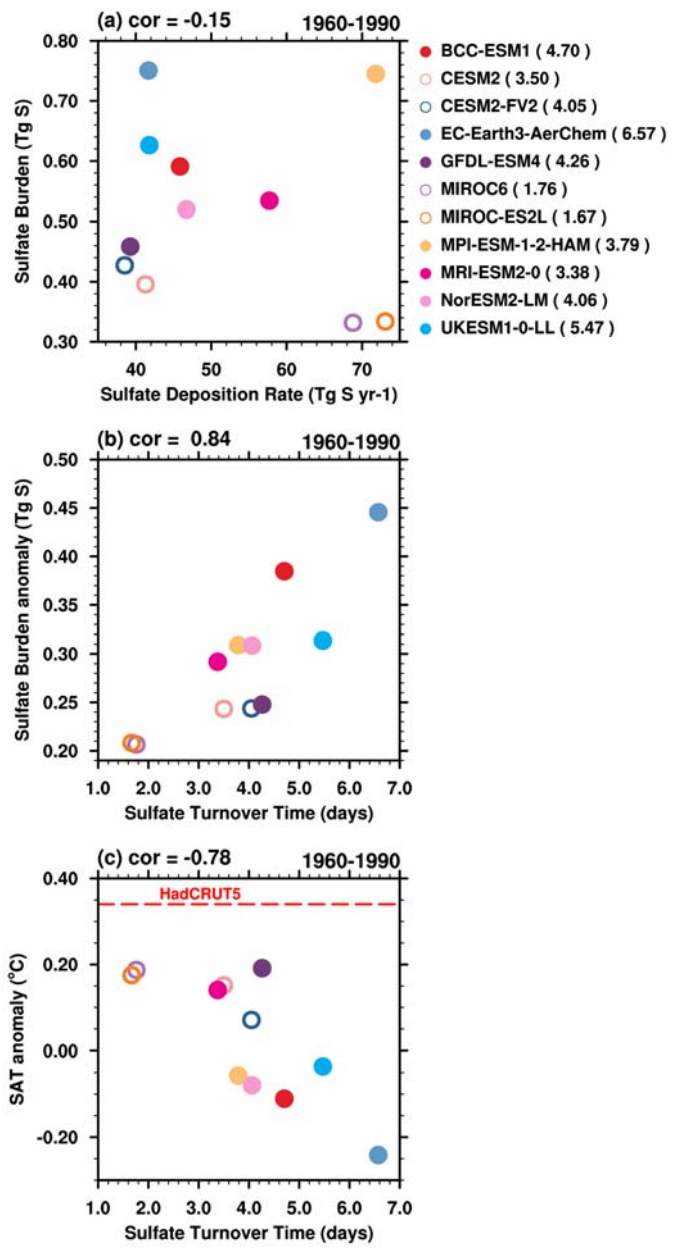

Figure 6. (a) Sulfate deposition versus sulfate burden during 1960-1990. (b) Sulfate turnover time versus sulfate burden anomaly during 1960-1990. (c) Sulfate turnover time versus SATa during 1960-1990.

Figure 6 presents the simulated sulfate deposition and sulfate burden in 1960-1990. The weak negative correlation (-0.15) indicates that sulfate deposition alone cannot fully explain inter-model differences in sulfate burden. Sulfate turnover time is quantified following Eq. (2) in Section 2.2 as the ratio of sulfate burden to sulfate deposition, representing the average atmospheric residence time of sulfate aerosols. The sulfate turnover time exhibits considerable inter-model variability, ranging from 1.67 days in MIROC-ES2L to 6.57 days in EC-Earth3-AerChem. These results generally agree with most aerosol models, which typically simulate sulfate lifetimes of around 4 days (e.g., Textor et al.,2006; Liu et al., 2012; Matsui and Mahowald, 2017; Tegen et al., 2019). However, sulfate turnover times in models are notably shorter than observational estimates, such as 7.3 days (0.02 yr) in Charlson et al. (1992) and 10-14 days in Kristiansen et al. (2012). This discrepancy may stem from premature removal processes, inadequate poleward transport, or incomplete chemical representations (e.g., Croft et al., 2014).

The inter-model variations in sulfate turnover time exhibit a strong correlation with sulfate burden anomalies and SATa during the 1960-1990 period, with a correlation coefficient of 0.84 and -0.78 (Fig.6b and Fig.6c). This suggests that differences in sulfate turnover time may account for both the sulfate burden anomaly variations and the consequent surface temperature differences among models. CMIP6 models systematically overestimate sulfate burden anomalies, implying that these models should exhibit shorter lifetimes to produce lower sulfate burden anomalies (Fig.6c). However, enhancing sulfate deposition to reduce burden anomalies is not a physically consistent solution, as it would worsen the already too-short simulated sulfate aerosol lifetime.

Therefore, as indicated by section 3.2, model improvement efforts should prioritize SO_2 deposition process refinement over sulfate deposition adjustments as a more scientifically sound approach.

3.4 The performances in the two post-CMIP6 models

To suppress the substantial cold bias in the BCC-ESM1 model, which underestimates the observed SATa by 0.45°C, we increase the dry deposition velocity of SO_2 by a factor of four over land surfaces and by a factor of 1.5 over the ocean to reduce the availability of SO_2 for oxidation. This effect is similar to that in UKESM1-0-LL by improving SO_2 dry deposition parameterization (Hardacre et al., 2021; Mulcahy et al., 2023). The impact of changes to the SO_2 dry deposition parameterization in UKESM1-0-LL is an increase of SO_2 dry deposition by a factor of 2 to 4. Accordingly, SATa increases to 0.45ºC in BCC-ESM1-1 and rises to 0.25ºC in UKESM1-LL. Sulfate turnover time in the two post-CMIP6 models, 8.53 days in BCC-ESM1-1 and 5.77 days in UKESM1-1-LL, is generally longer than that of their CMIP6 versions. The longer sulfate lifetimes in the two post-CMIP6 models may be due to lower SO_2 in these revised models, but also could be due to physical climate changes (e.g., temperatures, clouds, rainfall).

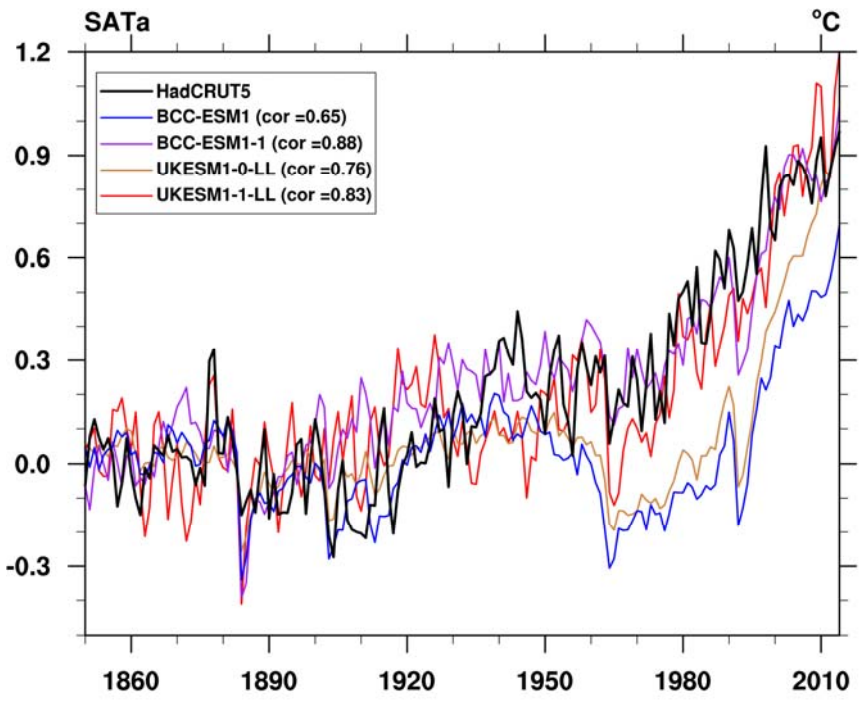

Figure 7. Evolutions of SATa relative to 1850-1900 mean for HadCRUT5, BCC-ESM models, and UKESM models. The numbers in legend are the corresponding correlation coefficients with HadCRUT5.

As demonstrated by the global mean SATa in BCC-ESM1-1 and UKESM1-1-LL models (Fig.7), both models on average tracked the instrumental record quite well with statistically higher correlation coefficients with observation (HadCRUT5). That is, improvements in SO_2 deposition parameterizations have contributed to better model performances in reproducing historical surface temperature evolution.

3.5 Relative changes preceding and following the 1960-1990 period

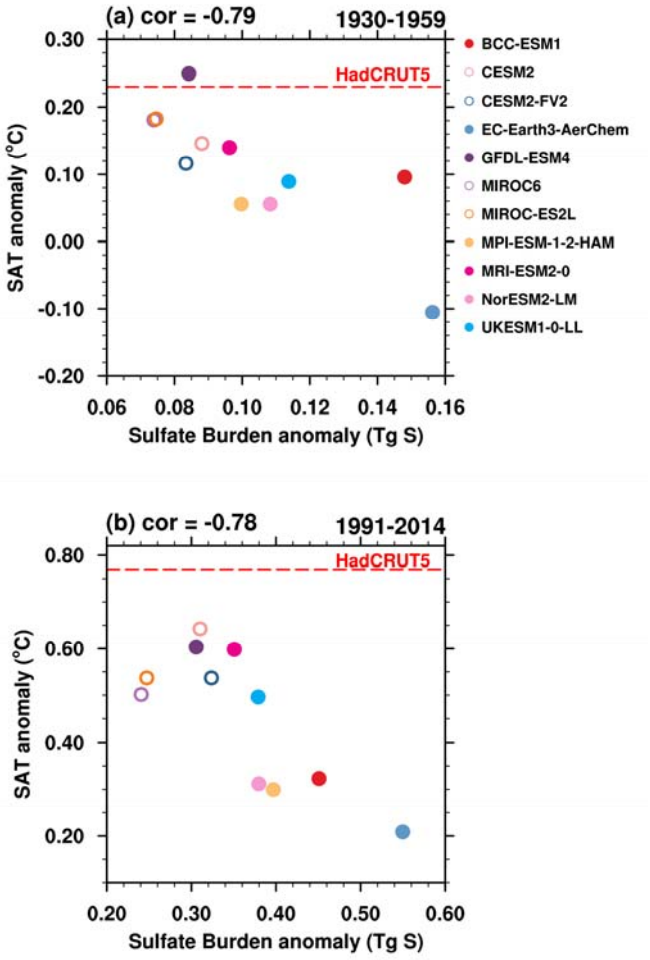

Figure 8. Correlate sulfate burden anomalies with SATa in (a) 1930-1959, and (b) 1991-2014.

Our analysis reveals a robust correlation between sulfate burden anomalies and SATa during 1960-1990 (Fig. 2a). To evaluate the temporal consistency of this relationship, we examined its behavior before and after this period. Given that the

relationship reflects clear underlying physics, similar correlations were expected across different periods. As shown in Fig.8, statistically significant correlations are evident in both periods, suggesting that sulfate burden anomalies were overestimated prior to 1960-1990, and this overestimation continued to influence SATa in subsequent decades. Compared to HadCRUT5, the models on average underestimates SATa by 0.11°C during 1930-1959 and by 0.31°C during 1991-2014. The correlations between sulfate burden anomalies and SATa are −0.79 and −0.78 for these two periods (Fig.8), respectively, which are weaker than the correlation of −0.91 during 1960-1990. This weakening may be partly attributable to the smaller biases in the 1930-1959 interval. Furthermore, the combined effects of increasing atmospheric CO_2 concentrations since the Industrial Revolution and the high climate sensitivity in CMIP6 models may have partially offset the cooling bias during 1991-2014 (Hausfather et al., 2022).

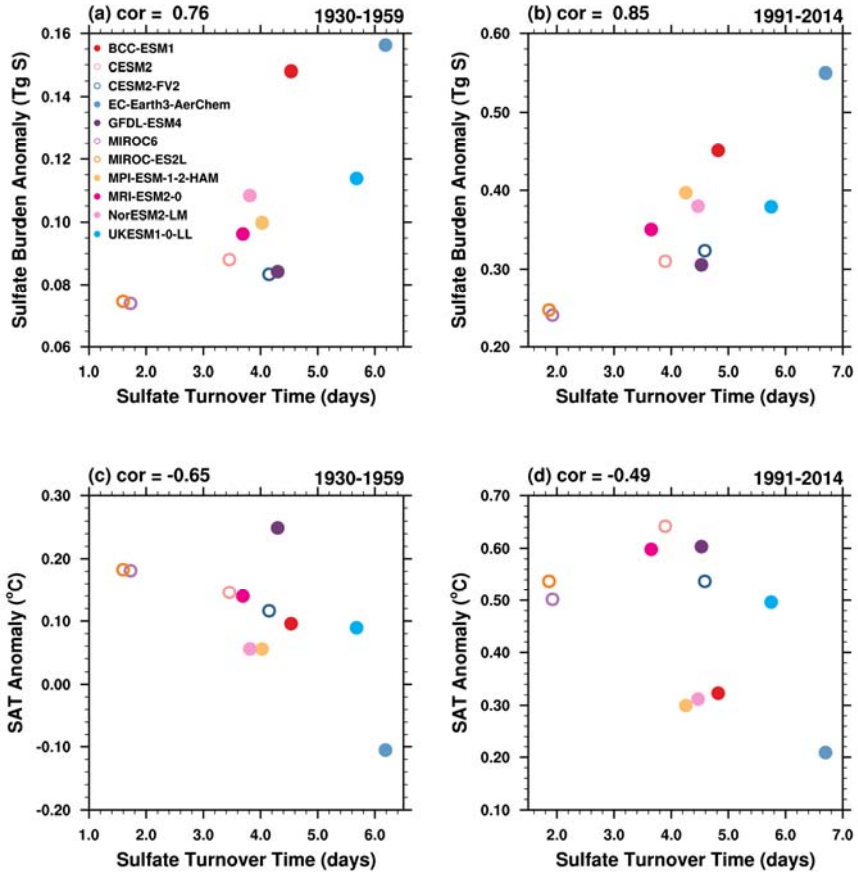

Figure 9. Correlation between sulfate turnover time (τ_{SO_4}) and: (a, b) sulfate burden anomalies, and (c, d) SATa for the periods 1930-1959 and 1991-2014.

Sulfate turnover time is a key parameter governing sulfate burden and shows strong correlations with sulfate burden anomalies and SATa during 1960-1990 (Figs. 6b and 6c). Statistically significant correlations persist before and after this period (Fig. 9), confirming the dominant role of sulfate-related physical processes across all examined time intervals.

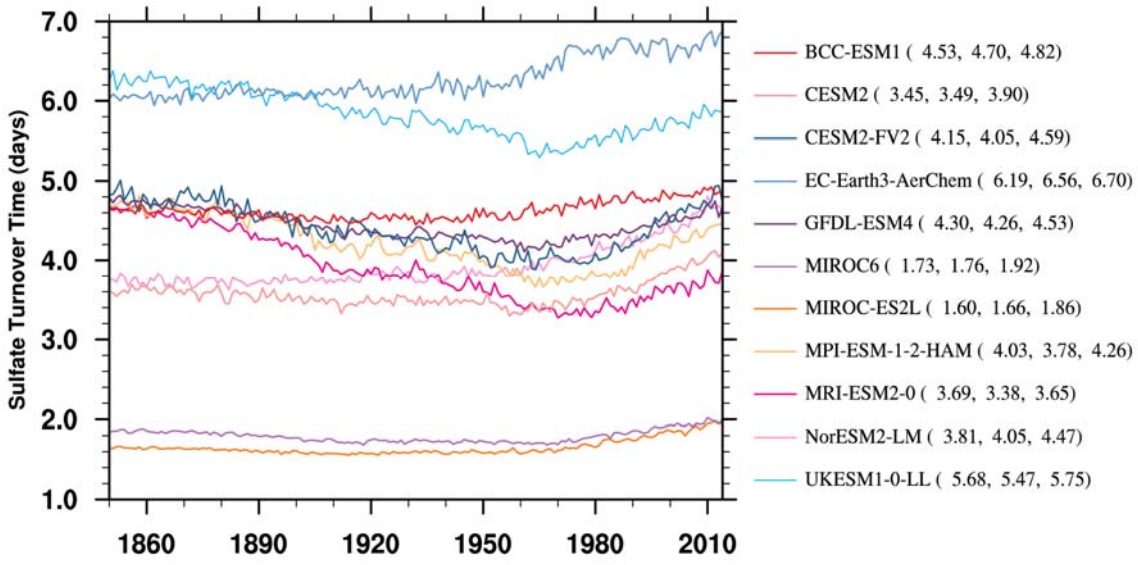

Figure 10. Temporal evolution of sulfate turnover time (τ_{SO_4}) in CMIP6 models. Numerical labels denote mean τ_{SO_4} value during 1930-1959, 1960-1990, and 1991-2014.

We also analyze the temporal evolution of sulfate turnover time (Fig.10). Its temporal variability, characterized by a standard deviation ($\sigma < 0.5$ days), is notably smaller than the inter-model spread. During 1930-1959, models exhibit divergent trend, with 5 out of 11 models simulating reduced turnover times in the subsequent period. In contrast, all models show prolonged turnover times during 1991-2014 compared to earlier periods. This shift may be partly attributable to changes in the regional distribution of sulfur emissions, including an increasing proportion of emissions from Asia and the implementation of stringent emission control policies in Europe and North America.

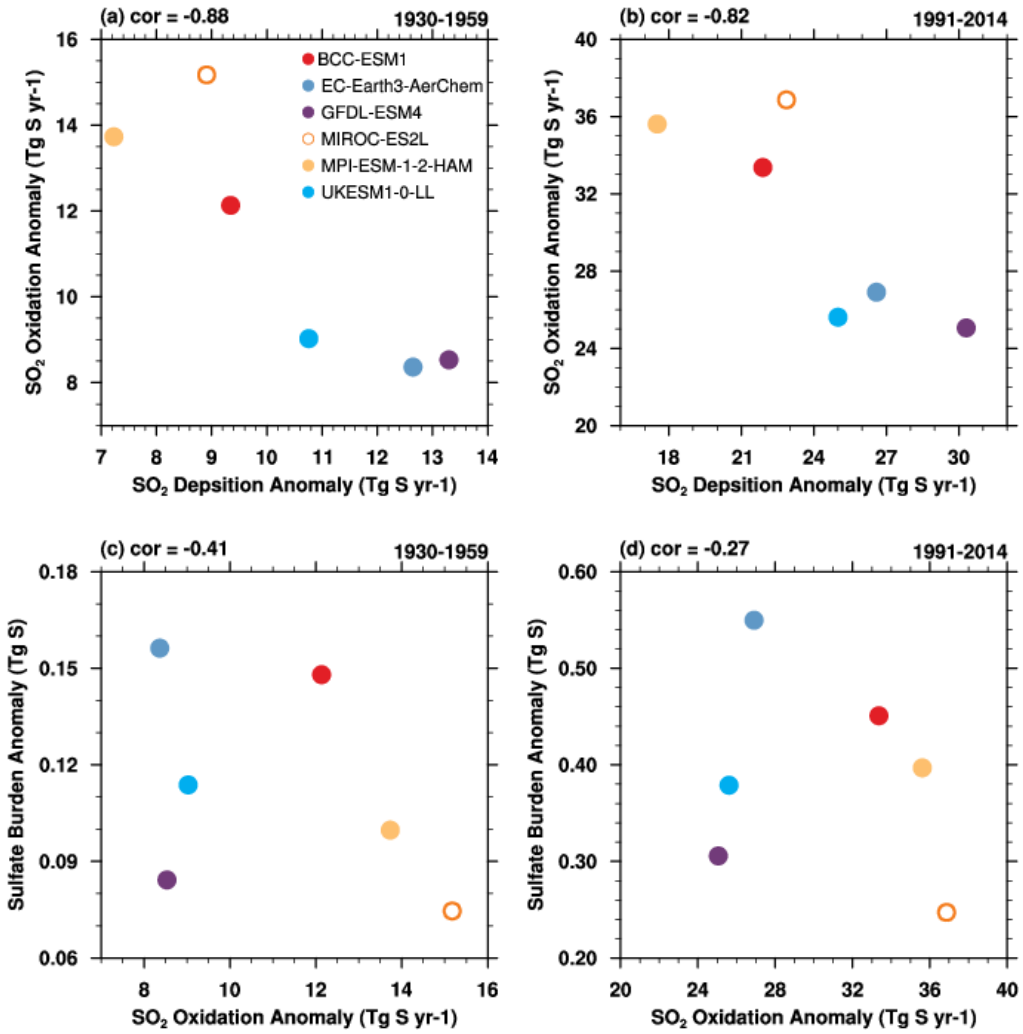

Figure 11. Same as Fig.4, but for (a, c) 1930-1959, and (b, d) 1991-2014.

The relationships among anomalies of SO_2 deposition, sulfate depositions, and SO_2 oxidation persist consistently over time (Fig.11). SO_2 deposition maintains a strong negative correlation with SO_2 oxidation both before and after the 1960-1990 period, with coefficients of −0.88 and −0.82, respectively. Meanwhile, the anomaly in SO_2 oxidation exhibits a negative but statistically insignificant correlation with sulfate burden anomaly.

4. Conclusions

The aerosol cooling effect is considered as the second most important anthropogenic forcing during the 20th Century. Based on the 11 CMIP6 models with

aerosol schemes, our study demonstrates that the cooling bias during 1960-1990 is closely related to the sulfate burden changes in the atmosphere. Sulfate aerosol represents the terminal product of a complex chain of physicochemical processes that convert sulfur emissions into sulfate particles. Our findings indicate that sulfate burden anomalies in these models are governed by two key processes: the removal of its gaseous precursor SO_2 and sulfate deposition itself. Higher SO_2 deposition rates limit the availability of SO_2 for subsequent oxidations. Sulfate turnover time is critical for evaluating the physical realism of models. Comparative analysis with observational measurements reveals that increasing sulfate deposition to reduce sulfate burden anomalies is not a reasonable approach. Biases in sulfate burden anomalies may be driven by discrepancies in simulating upstream SO_2 deposition and oxidation processes, rather than downstream processes. This is further supported by improvements in two post-CMIP6 models with refined SO_2 deposition parameterizations.

Analyses for periods preceding and following 1960-1990 confirm the persistent influence of sulfate-related physical processes across all examined time periods. Therefore, CMIP6 model projections should be interpreted with caution, as they may underestimate future warming rates. It is therefore also essential to evaluate the reliability of sulfate-related processes in upcoming model intercomparisons before applying them to future climate projections. We encourage future intercomparison initiatives to archive sulfur cycle relevant outputs from a wider range of participating models, thereby enabling more robust and comprehensive process-oriented evaluations.

Code availability

All data processing codes are available if a request is sent to the corresponding authors.

Data availability

The HadCRUT5 dataset is accessible through Met Office Hadley Centre observations database (https://www.metoffice.gov.uk/hadobs/hadcrut5/). All the model data can be freely downloaded from the Earth System Grid Federation (ESGF) nodes

(https://aims2.llnl.gov/search/cmip6/).

Author contributions

The main ideas were formulated by J.Z. and K.F. J.Z. wrote the original draft. The results were supervised by K.F. and S.T.T. All the authors discussed the results and contributed to the final manuscript.

Competing interests

The authors declare no competing financial and/or non-financial interests.

Acknowledgements

We sincerely appreciate the constructive and insightful comments from Dr. Stephen E. Schwartz and anonymous reviewers, which significantly improved the quality of this manuscript. We acknowledge all data developers, their managers, and funding agencies for the datasets used in this study, whose work and support are essential to us.

Financial support

This work was jointly supported by the National Natural Science Foundation of China (Grant no. U2542212 and 42230608) and the UK–China Research and Innovation Partnership Fund through the Met Office Climate Science for Service Partnership (CSSP) China as part of the Newton Fund.

References

Aas, W., Mortier, A., Bowersox, V., Cherian, R., Faluvegi, G., Fagerli, H., Hand, J., Klimont, Z., Galy-Lacaux, C., Lehmann, C. M. B., Myhre, C. L., Myhre, G., Olivié, D., Sato, K., Quaas, J., Rao, P. S. P., Schulz, M., Shindell, D., Skeie, R. B., Stein, A., Takemura, T., Tsyro, S., Vet, R., and Xu, X.: Global and regional trends of atmospheric sulfur, Scientific Reports, 9, 953, 10.1038/s41598-018-37304-0, 2019.

Bevacqua, E., Schleussner, C., and Zscheischler, J.: A year above 1.5 °C signals that Earth is most probably within the 20-year period that will reach the Paris Agreement limit, Nature Climate Change, 1-4, 10.1038/s41558-025-02246-9, 2025.

Charlson, R. J., Schwartz, S. E., Hales, J. M., Cess, R. D., Coakley, J. A., Hansen, J. E. and Hofmann, D. J.: Climate Forcing by Anthropogenic Aerosols, Science, 255, 423-430. 1992.

Chen, J. P., Chen, I. J. and Tsai, I. C.: Dynamic Feedback of Aerosol Effects on the East Asian Summer Monsoon, Journal of Climate, 29, 6137-6149. 2016.

Chin, M., Jacob, D. J., Gardner, G. M., Foreman-Fowler, M. S., Spiro, P. A. and Savoie, D. L.: A global three-dimensional model of tropospheric sulfate, Journal of Geophysical Research: Atmospheres, 101, 18667-18690. 1996.

Chylek, P., Folland, C., Klett, J. D., and Dubey, M. K.: CMIP5 Climate Models Overestimate Cooling by Volcanic Aerosols, Geophysical Research Letters, 47, e2020GL087047, https://doi.org/10.1029/2020GL087047, 2020.

Croft, B., Pierce, J. R. and Martin, R. V.: Interpreting aerosol lifetimes using the GEOS-Chem model and constraints from radionuclide measurements, Atmospheric Chemistry and Physics, 14, 4313-4325. 2014.

Danabasoglu, G., Lamarque, J. F., Bacmeister, J., Bailey, D. A., DuVivier, A. K., Edwards, J., Emmons, L. K., Fasullo, J., Garcia, R., Gettelman, A., Hannay, C., Holland, M. M., Large, W. G., Lauritzen, P. H., Lawrence, D. M., Lenaerts, J. T. M., Lindsay, K., Lipscomb, W. H., Mills, M. J., Neale, R., Oleson, K. W., Otto-Bliesner, B., Phillips, A. S., Sacks, W., Tilmes, S., van Kampenhout, L., Vertenstein, M., Bertini, A., Dennis, J., Deser, C., Fischer, C., Fox-Kemper, B., Kay, J. E., Kinnison, D., Kushner, P. J., Larson, V. E., Long, M. C., Mickelson, S., Moore, J.

K., Nienhouse, E., Polvani, L., Rasch, P. J., and Strand, W. G.: The Community Earth System Model Version 2 (CESM2), J. Adv. Model. Earth Syst., 12, 35, 10.1029/2019ms001916, 2020.

Dittus, A. J., Hawkins, E., Wilcox, L. J., Sutton, R. T., Smith, C. J., Andrews, M. B., and Forster, P. M.: Sensitivity of Historical Climate Simulations to Uncertain Aerosol Forcing, Geophysical Research Letters, 47, e2019GL085806, 10.1029/2019gl085806, 2020.

Döscher, R., Acosta, M., Alessandri, A., Anthoni, P., Arneth, A., Arsouze, T., Bergmann, T., Bernadello, R., Bousetta, S., Caron, L. P., Carver, G., Castrillo, M., Catalano, F., Cvijanovic, I., Davini, P., Dekker, E., Doblas-Reyes, F. J., Docquier, D., Echevarria, P., Fladrich, U., Fuentes-Franco, R., Gröger, M., v. Hardenberg, J., Hieronymus, J., Karami, M. P., Keskinen, J. P., Koenigk, T., Makkonen, R., Massonnet, F., Ménégoz, M., Miller, P. A., Moreno-Chamarro, E., Nieradzik, L., van Noije, T., Nolan, P., O'Donnell, D., Ollinaho, P., van den Oord, G., Ortega, P., Prims, O. T., Ramos, A., Reerink, T., Rousset, C., Ruprich-Robert, Y., Le Sager, P., Schmith, T., Schrödner, R., Serva, F., Sicardi, V., Sloth Madsen, M., Smith, B., Tian, T., Tourigny, E., Uotila, P., Vancoppenolle, M., Wang, S., Wårlind, D., Willén, U., Wyser, K., Yang, S., Yepes-Arbós, X., and Zhang, Q.: The EC-Earth3 Earth System Model for the Climate Model Intercomparison Project 6, Geosci. Model Dev. Discuss., 2021, 1-90, 10.5194/gmd-2020-446, 2021.

Dunne, J. P., Horowitz, L. W., Adcroft, A. J., Ginoux, P., Held, I. M., John, J. G., Krasting, J. P., Malyshev, S., Naik, V., Paulot, F., Shevliakova, E., Stock, C. A., Zadeh, N., Balaji, V., Blanton, C., Dunne, K. A., Dupuis, C., Durachta, J., Dussin, R., Gauthier, P. P. G., Griffies, S. M., Guo, H., Hallberg, R. W., Harrison, M., He, J., Hurlin, W., McHugh, C., Menzel, R., Milly, P. C. D., Nikonov, S., Paynter, D. J., Ploshay, J., Radhakrishnan, A., Rand, K., Reichl, B. G., Robinson, T., Schwarzkopf, D. M., Sentman, L. T., Underwood, S., Vahlenkamp, H., Winton, M., Wittenberg, A. T., Wyman, B., Zeng, Y., and Zhao, M.: The GFDL Earth System Model Version 4.1 (GFDL-ESM 4.1): Overall Coupled Model Description and Simulation Characteristics, J. Adv. Model. Earth Syst., 12, 10.1029/2019ms002015, 2020.

508 EB, U.: Protocol to Abate Acidification, Eutrophication and Ground-level Ozone, 1999.
509 Flynn, C. M. and Mauritsen, T.: On the climate sensitivity and historical warming
510 evolution in recent coupled model ensembles, Atmos. Chem. Phys., 20, 7829-7842,
511 10.5194/acp-20-7829-2020, 2020.
512 Hajima, T., Watanabe, M., Yamamoto, A., Tatebe, H., Noguchi, M. A., Abe, M.,
513 Ohgaito, R., Ito, A., Yamazaki, D., Okajima, H., Ito, A., Takata, K., Ogochi, K.,
514 Watanabe, S., and Kawamiya, M.: Development of the MIROC-ES2L Earth system
515 model and the evaluation of biogeochemical processes and feedbacks, Geoscientific
516 Model Development, 13, 2197-2244, 10.5194/gmd-13-2197-2020, 2020.
517 Hand, J. L., Schichtel, B. A., Malm, W. C., and Pitchford, M. L.: Particulate sulfate ion
518 concentration and SO_2 emission trends in the United States from the early 1990s
519 through 2010, Atmos. Chem. Phys., 12, 10353-10365, 10.5194/acp-12-10353-2012,
520 2012.
521 Hansen, J., Kharecha, P., Sato, M., Tselioudis, G., Kelly, J., Bauer, S., Ruedy, R., Jeong,
522 E., Jin, Q., Rignot, E., Velicogna, I., Schoeberl, M., Schuckmann, K., Amponsem,
523 J., Cao, J., Keskinen, A., Li, J., and Pokela, A.: Global Warming Has Accelerated:
524 Are the United Nations and the Public Well-Informed?, Environment: Science and
525 Policy for Sustainable Development, 67, 6-44, 10.1080/00139157.2025.2434494,
526 2025.
527 Hardacre, C., Mulcahy, J. P., Pope, R. J., Jones, C. G., Rumbold, S. T., Li, C., Johnson,
528 C., and Turnock, S. T.: Evaluation of SO_2, SO_4^{2-} and an updated SO_2 dry deposition
529 parameterization in the United Kingdom Earth System Model, Atmospheric
530 Chemistry and Physics, 21, 18465-18497, 10.5194/acp-21-18465-2021, 2021.
531 Hausfather, Z., Marvel, K., Schmidt, G. A., Nielsen-Gammon, J. W. and Zelinka, M.:
532 Climate simulations: recognize the 'hot model' problem, Nature, 605, 26-29. 2022.
533 Hegerl, G.C., F. W. Zwiers, P. Braconnot, N.P. Gillett, Y. Luo, J.A. Marengo Orsini,
534 N. Nicholls, J.E. Penner and P.A. Stott, 2007: Understanding and Attributing
535 Climate Change. In: Climate Change 2007: The Physical Science Basis.
536 Contribution of Working Group I to the Fourth Assessment Report of the
537 Intergovernmental Panel on Climate Change [Solomon, S., D. Qin, M. Manning, Z.

538 Chen, M. Marquis, K.B. Averyt, M. Tignor and H.L. Miller (eds.)]. Cambridge
539 University Press, Cambridge, United Kingdom and New York, NY, USA.
540 Held, I. M., Winton, M., Takahashi, K., Delworth, T., Zeng, F. R. and Vallis, G. K.:
541 Probing the Fast and Slow Components of Global Warming by Returning Abruptly
542 to Preindustrial Forcing, Journal of Climate, 23, 2418-2427. 2010.
543 Hienola, A., Partanen, A.-I., Pietikäinen, J.-P., O'Donnell, D., Korhonen, H., Matthews,
544 H. D., and Laaksonen, A.: The impact of aerosol emissions on the 1.5 °C pathways,
545 Environmental Research Letters, 13, 044011, 10.1088/1748-9326/aab1b2, 2018.
546 Hoesly, R. M., Smith, S. J., Feng, L., Klimont, Z., Janssens-Maenhout, G., Pitkanen,
547 T., Seibert, J. J., Vu, L., Andres, R. J., Bolt, R. M., Bond, T. C., Dawidowski, L.,
548 Kholod, N., Kurokawa, J. I., Li, M., Liu, L., Lu, Z., Moura, M. C. P., O'Rourke, P.
549 R., and Zhang, Q.: Historical (1750–2014) anthropogenic emissions of reactive
550 gases and aerosols from the Community Emissions Data System (CEDS), Geosci.
551 Model Dev., 11, 369-408, 10.5194/gmd-11-369-2018, 2018.
552 IPCC. Climate Change 2021 – The Physical Science Basis: Working Group I
553 Contribution to the Sixth Assessment Report of the Intergovernmental Panel on
554 Climate Change, 10.1017/9781009157896, 2023.
555 Kristiansen, N. I., Stohl, A. and Wotawa, G.: Atmospheric removal times of the aerosol-
556 bound radionuclides ^{137}Cs and ^{131}I measured after the Fukushima Dai-ichi nuclear
557 accident – a constraint for air quality and climate models, Atmos. Chem.
558 Phys., 12, 10759-10769. 2012.
559 Likens, G. E., Butler, T. J., and Buso, D. C.: Long- and short-term changes in sulfate
560 deposition: Effects of the 1990 Clean Air Act Amendments, Biogeochemistry, 52,
561 1-11, 10.1023/a:1026563400336, 2001.
562 Liu, X., Easter, R. C., Ghan, S. J., Zaveri, R., Rasch, P., Shi, X., Lamarque, J. F.,
563 Gettelman, A., Morrison, H., Vitt, F., Conley, A., Park, S., Neale, R., Hannay, C.,
564 Ekman, A. M. L., Hess, P., Mahowald, N., Collins, W., Iacono, M. J., Bretherton,
565 C. S., Flanner, M. G. and Mitchell, D.: Toward a minimal representation of aerosols
566 in climate models: description and evaluation in the Community Atmosphere Model
567 CAM5, Geoscientific Model Development, 5, 709-739. 2012.

568 Matsui, H. and Mahowald, N.: Development of a global aerosol model using a two-
569 dimensional sectional method: 2. Evaluation and sensitivity simulations, Journal of
570 Advances in Modeling Earth Systems, 9, 1887-1920. 2017.
571 Mauritsen, T., Bader, J., Becker, T., Behrens, J., Bittner, M., Brokopf, R., Brovkin, V.,
572 Claussen, M., Crueger, T., Esch, M., Fast, I., Fiedler, S., Flaeschner, D., Gayler, V.,
573 Giorgetta, M., Goll, D. S., Haak, H., Hagemann, S., Hedemann, C., Hohenegger, C.,
574 Ilyina, T., Jahns, T., Jimenez-de-la-Cuesta, D., Jungclaus, J., Kleinen, T., Kloster,
575 S., Kracher, D., Kinne, S., Kleberg, D., Lasslop, G., Kornblueh, L., Marotzke, J.,
576 Matei, D., Meraner, K., Mikolajewicz, U., Modali, K., Moebis, B., Muellner, W. A.,
577 Nabel, J. E. M. S., Nam, C. C. W., Notz, D., Nyawira, S.-S., Paulsen, H., Peters, K.,
578 Pincus, R., Pohlmann, H., Pongratz, J., Popp, M., Raddatz, T. J., Rast, S., Redler,
579 R., Reick, C. H., Rohrschneider, T., Schemann, V., Schmidt, H., Schnur, R.,
580 Schulzweida, U., Six, K. D., Stein, L., Stemmler, I., Stevens, B., von Storch, J.-S.,
581 Tian, F., Voigt, A., Vrese, P., Wieners, K.-H., Wilkenskjeld, S., Winkler, A., and
582 Roeckner, E.: Developments in the MPI-M Earth System Model version 1.2 (MPI-
583 ESM1.2) and Its Response to Increasing CO2, J. Adv. Model. Earth Syst., 11, 998-
584 1038, 10.1029/2018ms001400, 2019.
585 Morice, C. P., Kennedy, J. J., Rayner, N. A., Winn, J. P., Hogan, E., Killick, R. E.,
586 Dunn, R. J. H., Osborn, T. J., Jones, P. D., and Simpson, I. R.: An Updated
587 Assessment of Near-Surface Temperature Change From 1850: The HadCRUT5
588 Data Set, Journal of Geophysical Research-Atmospheres, 126,
589 10.1029/2019jd032361, 2021.
590 Mulcahy, J. P., Jones, C. G., Rumbold, S. T., Kuhlbrodt, T., Dittus, A. J., Blockley, E.
591 W., Yool, A., Walton, J., Hardacre, C., Andrews, T., Bodas-Salcedo, A., Stringer,
592 M., de Mora, L., Harris, P., Hill, R., Kelley, D., Robertson, E., and Tang, Y.:
593 UKESM1.1: development and evaluation of an updated configuration of the UK
594 Earth System Model, Geosci. Model Dev., 16, 1569-1600, 10.5194/gmd-16-1569-
595 2023, 2023.
596 Mulcahy, J. P., Johnson, C., Jones, C. G., Povey, A. C., Scott, C. E., Sellar, A., Turnock,
597 S. T., Woodhouse, M. T., Abraham, N. L., Andrews, M. B., Bellouin, N., Browse,

598 J., Carslaw, K. S., Dalvi, M., Folberth, G. A., Glover, M., Grosvenor, D. P.,
599 Hardacre, C., Hill, R., Johnson, B., Jones, A., Kipling, Z., Mann, G., Mollard, J.,
600 O'Connor, F. M., Palmieri, J., Reddington, C., Rumbold, S. T., Richardson, M.,
601 Schutgens, N. A. J., Stier, P., Stringer, M., Tang, Y., Walton, J., Woodward, S., and
602 Yool, A.: Description and evaluation of aerosol in UKESM1 and HadGEM3-GC3.1
603 CMIP6 historical simulations, Geoscientific Model Development, 13, 6383-6423,
604 10.5194/gmd-13-6383-2020, 2020.
605 O'Neill, B. C., Tebaldi, C., van Vuuren, D. P., Eyring, V., Friedlingstein, P., Hurtt, G.,
606 Knutti, R., Kriegler, E., Lamarque, J. F., Lowe, J., Meehl, G. A., Moss, R., Riahi,
607 K., and Sanderson, B. M.: The Scenario Model Intercomparison Project
608 (ScenarioMIP) for CMIP6, Geosci. Model Dev., 9, 3461-3482, 10.5194/gmd-9-
609 3461-2016, 2016.
610 Ohara, T., Akimoto, H., Kurokawa, J., Horii, N., Yamaji, K., Yan, X., and Hayasaka,
611 T.: An Asian emission inventory of anthropogenic emission sources for the period
612 1980-2020, Atmospheric Chemistry and Physics, 7, 4419-4444, 10.5194/acp-7-
613 4419-2007, 2007.
614 Samset, B. H., Sand, M., Smith, C. J., Bauer, S. E., Forster, P. M., Fuglestvedt, J. S.,
615 Osprey, S., and Schleussner, C.-F.: Climate Impacts From a Removal of
616 Anthropogenic Aerosol Emissions, Geophysical Research Letters, 45, 1020-1029,
617 https://doi.org/10.1002/2017GL076079, 2018.
618 Seland, Ø., Bentsen, M., Olivié, D., Toniazzo, T., Gjermundsen, A., Graff, L. S.,
619 Debernard, J. B., Gupta, A. K., He, Y. C., Kirkevåg, A., Schwinger, J., Tjiputra, J.,
620 Aas, K. S., Bethke, I., Fan, Y., Griesfeller, J., Grini, A., Guo, C., Ilicak, M., Karset,
621 I. H. H., Landgren, O., Liakka, J., Moseid, K. O., Nummelin, A., Spensberger, C.,
622 Tang, H., Zhang, Z., Heinze, C., Iversen, T., and Schulz, M.: Overview of the
623 Norwegian Earth System Model (NorESM2) and key climate response of CMIP6
624 DECK, historical, and scenario simulations, Geosci. Model Dev., 13, 6165-6200,
625 10.5194/gmd-13-6165-2020, 2020.
626 Sellar, A. A., Jones, C. G., Mulcahy, J. P., Tang, Y., Yool, A., Wiltshire, A., O'Connor,
627 F. M., Stringer, M., Hill, R., Palmieri, J., Woodward, S., de Mora, L., Kuhlbrodt, T.,

Rumbold, S. T., Kelley, D. I., Ellis, R., Johnson, C. E., Walton, J., Abraham, N. L., Andrews, M. B., Andrews, T., Archibald, A. T., Berthou, S., Burke, E., Blockley, E., Carslaw, K., Dalvi, M., Edwards, J., Folberth, G. A., Gedney, N., Griffiths, P. T., Harper, A. B., Hendry, M. A., Hewitt, A. J., Johnson, B., Jones, A., Jones, C. D., Keeble, J., Liddicoat, S., Morgenstern, O., Parker, R. J., Predoi, V., Robertson, E., Siahaan, A., Smith, R. S., Swaminathan, R., Woodhouse, M. T., Zeng, G., and Zerroukat, M.: UKESM1: Description and Evaluation of the UK Earth System Model, J. Adv. Model. Earth Syst., 11, 4513-4558, 10.1029/2019ms001739, 2019.

Smith, C. J. and Forster, P. M.: Suppressed Late-20th Century Warming in CMIP6 Models Explained by Forcing and Feedbacks, Geophysical Research Letters, 48, 10.1029/2021gl094948, 2021.

Steffen, W., Crutzen, P. J., and McNeill, J. R.: The Anthropocene: Are humans now overwhelming the great forces of nature, Ambio, 36, 614-621, 10.1579/0044-7447(2007)36[614:taahno]2.0.co;2, 2007.

Tatebe, H., Ogura, T., Nitta, T., Komuro, Y., Ogochi, K., Takemura, T., Sudo, K., Sekiguchi, M., Abe, M., Saito, F., Chikira, M., Watanabe, S., Mori, M., Hirota, N., Kawatani, Y., Mochizuki, T., Yoshimura, K., Takata, K., O'Ishi, R., Yamazaki, D., Suzuki, T., Kurogi, M., Kataoka, T., Watanabe, M., and Kimoto, M.: Description and basic evaluation of simulated mean state, internal variability, and climate sensitivity in MIROC6, Geoscientific Model Development, 12, 2727-2765, 10.5194/gmd-12-2727-2019, 2019.

Tegen, I., Neubauer, D., Ferrachat, S., Siegenthaler-Le Drian, C., Bey, I., Schutgens, N., Stier, P., Watson-Parris, D., Stanelle, T., Schmidt, H., Rast, S., Kokkola, H., Schultz, M., Schroeder, S., Daskalakis, N., Barthel, S., Heinold, B. and Lohmann, U.: The global aerosol-climate model ECHAM6.3-HAM2.3-Part 1: Aerosol evaluation, Geoscientific Model Development, 12, 1643-1677. 2019.

Textor, C., Schulz, M., Guibert, S., Kinne, S., Balkanski, Y., Bauer, S., Berntsen, T., Berglen, T., Boucher, O., Chin, M., Dentener, F., Diehl, T., Easter, R., Feichter, H., Fillmore, D., Ghan, S., Ginoux, P., Gong, S., Kristjansson, J. E., Krol, M., Lauer, A., Lamarque, J. F., Liu, X., Montanaro, V., Myhre, G., Penner, J., Pitari, G., Reddy,

S., Seland, O., Stier, P., Takemura, T. and Tie, X.: Analysis and quantification of the diversities of aerosol life cycles within AeroCom, Atmospheric Chemistry and Physics, 6, 1777-1813. 2006.

Vestreng, V., Myhre, G., Fagerli, H., Reis, S., and Tarrasón, L.: Twenty-five years of continuous sulphur dioxide emission reduction in Europe, Atmos. Chem. Phys., 7, 3663-3681, 10.5194/acp-7-3663-2007, 2007.

Wang, Z., Lin, L., Xu, Y., Che, H., Zhang, X., Zhang, H., Dong, W., Wang, C., Gui, K., and Xie, B.: Incorrect Asian aerosols affecting the attribution and projection of regional climate change in CMIP6 models, Npj Climate and Atmospheric Science, 4, 10.1038/s41612-020-00159-2, 2021.

Watterson, I. G. and Dix, M. R.: Effective sensitivity and heat capacity in the response of climate models to greenhouse gas and aerosol forcings, Quarterly Journal of the Royal Meteorological Society, 131, 259-279. 2005.

Wilcox, L. J., Highwood, E. J., and Dunstone, N. J.: The influence of anthropogenic aerosol on multi-decadal variations of historical global climate, Environmental Research Letters, 8, 10.1088/1748-9326/8/2/024033, 2013.

Wu, T., Zhang, F., Zhang, J., Jie, W., Zhang, Y., Wu, F., Li, L., Yan, J., Liu, X., Lu, X., Tan, H., Zhang, L., Wang, J., and Hu, A.: Beijing Climate Center Earth System Model version 1 (BCC-ESM1): model description and evaluation of aerosol simulations, Geosci. Model Dev., 13, 977-1005, 10.5194/gmd-13-977-2020, 2020.

Yukimoto, S., Kawai, H., Koshiro, T., Oshima, N., Yoshida, K., Urakawa, S., Tsujino, H., Deushi, M., Tanaka, T., Hosaka, M., Yabu, S., Yoshimura, H., Shindo, E., Mizuta, R., Obata, A., Adachi, Y., and Ishii, M.: The Meteorological Research Institute Earth System Model Version 2.0, MRI-ESM2.0: Description and Basic Evaluation of the Physical Component, Journal of the Meteorological Society of Japan, 97, 931-965, 10.2151/jmsj.2019-051, 2019.

Zhang, J., Furtado, K., Turnock, S. T., Mulcahy, J. P., Wilcox, L. J., Booth, B. B., Sexton, D., Wu, T., Zhang, F., and Liu, Q.: The role of anthropogenic aerosols in the anomalous cooling from 1960 to 1990 in the CMIP6 Earth System Models, Atmos. Chem. Phys. Discuss., 1-39, 10.5194/acp-2021-570, 2021a.

688 Zhang, J., Wu, T., Zhang, F., Furtado, K., Xin, X., Shi, X., Li, J., Chu, M., Zhang, L.,
689 Liu, Q., Yan, J., Wei, M., and Ma, Q.: BCC-ESM1 Model Datasets for the CMIP6
690 Aerosol Chemistry Model Intercomparison Project (AerChemMIP), Advances in
691 Atmospheric Sciences, 38, 317-328, 10.1007/s00376-020-0151-2, 2021b.